CCS Chemistry

COMMUNICATION

Received: Nov. 13, 2021 | Accepted: Jan. 26, 2022 | Published: Feb. 25, 2022

Stable Metal–Halide Perovskite Colloids in Protic Ionic Liquid

Hao Gu[1,2†], Tingting Niu[3†], Shouwei Zuo[4,5†], Yongqing Cai[2†], Lingfeng Chao[3], Peter Müller-Buschbaum[6,7], Yingdong Xia[1], Jing Zhang[4,5], Guichuan Xing[2] & Yonghua Chen[1*]

[1]*Key Laboratory of Flexible Electronics (KLOFE), Institution of Advanced Materials (IAM), Nanjing Tech University (NanjingTech), Nanjing 211816, Jiangsu,* [2]*Joint Key Laboratory of the Ministry of Education, Institute of Applied Physics and Materials Engineering, University of Macau, Taipa 999078, Macau,* [3]*Frontiers Science Center for Flexible Electronics, Xi'an Institute of Flexible Electronics (IFE), Xi'an Institute of Biomedical Materials & Engineering, Northwestern Polytechnical University, Xi'an 710072,* [4]*Beijing Synchrotron Radiation Facility, Institute of High Energy Physics, Chinese Academy of Sciences, Beijing 100049,* [5]*University of Chinese Academy of Sciences, Beijing 100049,* [6]*Lehrstuhl für Funktionelle Materialien, Physik Department, Technische Universität München, Garching 85748,* [7]*Heinz Maier-Leibnitz Zentrum (MLZ), Technische Universität München, Garching 85748*

**Corresponding author: iamyhchen@njtech.edu.cn;* †H. Gu, T. Niu, S. Zuo, and Y. Cai contributed equally to this work.

Cite this: *CCS Chem.* **2022**, 4, 3264–3274
DOI: 10.31635/ccschem.022.202101629

Obtaining long-term stable and robust perovskite colloids solution remains an important scientific challenge due to the limited interaction between solvent and perovskite solutes. Here, we unveil the formation mechanism of chemically robust perovskite precursor solutions under ambient conditions using methylammonium acetate (CH_3NH_3•CH_3COO, MAAc) protic ionic liquid (PIL) solvent. Tens of nanometers colloids are assembled on the molecular level via regular oriented gel-like lamellae with a mean thickness of 34.69 nm, width of 56.81 nm, and distance of 91.05 nm. Stable colloids could be realized in the MAAc precursor solution with uniform distribution through N–H•••O=C–O^- intermolecular hydrogen bonds and the O=C–O^- (Ac^-) and Pb^{2+} coordination interactions, in which the coordination number of Pb^{2+} ions increased slightly from 1.6 ± 0.2 to 1.7 ± 0.4 as the MAAc precursor concentration increased, leading to the Pb–O scattering distance of only 1.7 Å in the R space. Moreover, first-principles molecular dynamics simulations also demonstrate that the Ac^- anions can promote the formation and stabilization of precursor solutions. These interactions yielded more stable perovskite colloids precursors solutions compared to traditional *N*,*N*-dimethylformamide and dimethyl sulfoxide solution under heat stress, air aging, and electrolytic dissociation. The abundant varieties of robust PIL solvents could potentially facilitate the success of many perovskite-based optoelectronic devices.

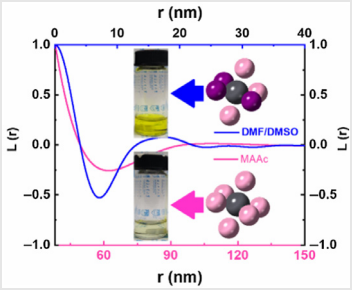

We reveal the truth of perovskite precursor colloids chemically robust and long-term processing ability, by unveiling the assemble formation and coordination interaction between protic ionic liquid (PIL) and perovskite solutes. The resulting understanding motivates us to use and develop various robust PIL solvents, which potentially facilitate the success of many perovskite-based optoelectronic devices.

Keywords: perovskite colloids, protic ionic liquid, X-ray absorption fine structure spectroscopy, coordination interaction

DOI: 10.31635/ccschem.022.202101629
Citation: *CCS Chem.* **2022**, 4, 3264–3274
Link to VoR: https://doi.org/10.31635/ccschem.022.202101629

Introduction

The metal–halide perovskites are promising candidate materials for use in high-performance photovoltaics, light-emitting diodes (LEDs), lasers, detectors, field-effect transistors, and other optoelectronic devices due to their superior physical and electronic properties.[1–11] These achievements have been realized through the solution processability of perovskites materials, where the metal halide salts are dissolved in aprotic polar solvents by coordination interactions, hydrogen-bonding effects, Lewis acid–base intermediates, and so on.[12–17] So, a robust perovskite precursor solution, which contains stable colloid particles in a mother solution of dissolved ions, is important to obtaining high-quality thin films and single crystals.[18,19] Currently, the limitation of precursor solution chemistry stems from the limited solubility of metal halides in the most used common solvents of *N*,*N*-dimethylformamide (DMF) and dimethyl sulfoxide (DMSO). The weak coordination interaction between Lewis acid, for example, PbI_2, and Lewis base, for example, DMF or DMSO, highly limits the stability of perovskite colloids.[15,16] The antisolvent method must be performed in a glovebox for the DMF/DMSO precursor solution.[17–19] This has hindered the reproducibility and potential mass production of stable and robust perovskites. In the case of a methylammonium acetate (MAAc) precursor solution, the perovskite films were prepared regardless of humidity by a simple one-step method without an antisolvent treatment or air-processing approach.[20,21] Therefore, the discovery of robust solvents and colloidally stabilized precursors are important in the commercialization of solution-processed perovskite-based photophysical and optoelectronic devices.

Here, we report stable metal halide perovskite colloids in the protic ionic liquid (PIL) MAAc. We found that tens of nanometers colloids are assembled on the molecular level through regular oriented gel-like lamellae with a mean thickness of 34.69 nm, width of 56.81 nm, and mean distance of 91.05 nm. Chemically robust perovskite colloids were obtained through forming N–H•••O=C–O^- intermolecular hydrogen bonds and the O=C–O^- (Ac^-) and Pb^{2+} coordination interactions with Pb–O distance of only 1.68 ± 0.01 Å, which has been suggested to be difficult in traditional DMF or DMSO solvents. The Pb–I bonds were totally replaced by more stable Pb–O bonds, whereas the isolated I^- were protected through the formation of N–H•••I^- hydrogen bonds, which allow stable colloids even under heat stress, air aging, and electrolytic dissociation conditions. Furthermore, first-principles molecular dynamics (MDs) simulations reveal that the Ac^- anions can promote the formation and stabilization of precursor colloids solution. Up to nine perovskite components, including organic-inorganic hybrid perovskites, all-inorganic perovskites, and tin-based perovskites, were systematically investigated with serious degradation in the DMF/DMSO solution in just a few hours, while no visible changes in the MAAc solution was found up to several days. Moreover, highly stable colloids were generated in nine more PILs even after one-month air aging. Therefore, understanding the gelation processes of perovskite precursors in solvents could lay a foundation for improving colloidal stability and device performance.

Experimental Methods

Materials

Methylammonium iodide (MAI, 99.9%) and all other amine hydroiodates and hydrobromates were purchased from Advanced Election Technology Co., Ltd. (Yingkou, China). Lead iodide (PbI_2, 99.99%), cesium iodide (99.8%) and stannous iodide (99.9%) were purchased from TCI Development Co., Ltd. (Shanghai, China). Acetonitrile (ACN, 99.8% anhydrous), DMF (99.99%), DMSO (99.5%), chlorobenzene (99.9% anhydrous), ethanol (EtOH, 99.9% anhydrous), acetone, isopropanol (IPA, 99.9% anhydrous), acetic acid (HAc, 99.99%), and other aliphatic acids were used as received from Sigma Aldrich Trading Co., Ltd. (Shanghai, China). The methylamine solution (~40 wt % in H_2O) and any other amine solution were all purchased from Aladdin Biochemical Technology Co., Ltd. (Shanghai, China). Unless otherwise noted, all the reagents were used without additional treatment.

Synthesis of protic ionic liquids

HAc (57.6 mL) and methylamine solution (180 mL) were stirred in a 500 mL round bottom flask in an ice water bath for 2 h. After stirring at 0 °C for 2 h, the resultant solution was recovered by reduced pressure rotary evaporation at 65 °C for 1 h to produce synthesized PIL MAAc. The liquid product was put into a refrigerator for 2 h to crystallize. The solid powder was rinsed three times with diethyl ether and then dissolved in absolute ethanol. Then, the resultant solution was recovered by rotary evaporation at 65 °C for 1 h again. Finally, the liquid products were cooled to room temperature before use. The ionic liquids family, including methylammonium formate, MAAc, methylammonium propionate, ethylammonium acetate, propylammonium acetate, *n*-butylammonium acetate, butylammonium propionate, butylammonium butyric, pentammonium acetate, and hexammonium acetate, all have the similar optimized synthesis process.

Preparation of perovskite precursors

To prepare the $MAPbI_3$ precursor solution, MAI and PbI_2 powder were dissolved in DMF/DMSO (volume ratio is 4:1) and PIL solvents. The obtained precursor solutions were stirred at 65 °C for 2 h in an inert-atmosphere

DOI: 10.31635/ccschem.022.202101629
Citation: *CCS Chem.* **2022**, 4, 3264–3274
Link to VoR: https://doi.org/10.31635/ccschem.022.202101629

glovebox. The precursor concentration for Fourier transform infrared spectroscopy (FTIR), nuclear magnetic resonance (NMR) spectroscopy, and thermogravimetric analysis (TGA) was 1.2 M (DMF/DMSO) and 0.6 M (MAAc); the precursor concentration for the aging test and electrochemical measurement was 0.2 M; for small-angle X-ray scattering (SAXS) and X-ray absorption fine structure spectroscopy (XAFS) the concentration was 0.2, 0.3, and 0.4 M, respectively; for UV–visible absorption spectroscopy and photoluminescence mapping, the precursor concentration was 1×10^{-4} M. We denoted 0.2, 0.3, and 0.4 M as 02, 03, and 04 in the article.

Characterizations

The crystal structure was measured on a Rigaku (Smart Lab 3kW) X-ray diffractometer (Rigaku Co., Ltd., Tokyo, Tokushima) (Cu Ka radiation, λ = 1.5406 Å) under the operation conditions of 40 kV and 30 mA at test speed of 0.02 per step. UV–vis–NIR absorption spectra were conducted on a Shimadzu UV 1750 spectrophotometer (Shimadzu Corp., Kyoto, Japan). The photoluminescence (PL) mapping (3D scan mode) characterization was carried out on the FL7100 Fluorescence spectrophotometer (HITACHI Instruments Co. Ltd., Shanghai, China). The excitation wavelength was in the range of 200–450 nm and the monitoring window was 450–650 nm. Dynamic light scattering measurements were conducted by a Zetasizer Nano 55 ZS instrument (Malvern Panalytical Co., Ltd., Shanghai, China) with a 633 nm He-Ne laser. The X-ray photoelectron spectroscopy (XPS) measurement was performed on a PHI Versa Probe III scanning XPS microscope (ULVAC-PHI, Inc., Kanagawa, Japan) with monochromatic Al K-alpha X-ray source (1468 eV).

Results and Discussion

Stable perovskite colloids precursor solution behaviors

Considering the stability and performance of ionic liquids in comparison to traditional solvents, we aimed to discover the molecular assembling mechanism of PIL that could potentially coordinate with metal ions and be firmly surrounded with intermolecular hydrogen bonds in a robust precursor solution. Here, we sequentially observed the colloidal behavior of different compositional perovskite precursors ($MAPbI_3$, $FAPbI_3$, $Cs_{0.05}FA_{0.95}PbI_3$, $CsPbI_3$, $FA_{0.85}MA_{0.15}PbI_{2.55}Br_{0.45}$, $BA_2MA_3Pb_4I_{13}$, $MASnI_3$, $FASnI_3$, and $CsSnI_3$) in DMF/DMSO and organic PIL MAAc solvent under continuous aging in an ambient environment (Figure 1 and Supporting Information Figure S1) and continuous heat stress (Supporting Information Figure S2). We noticed a significant change in the pellucidity and color as the precursors became turbid and dark, indicating that they had deteriorated, for example, through the oxidation of Sn^{2+} and decomposition of formamidinium.[22–24] Particularly, after adding additional solvents, such as IPA, ACN, EtOH, and water (H_2O), the DMF/DMSO precursors foamed immediately, became highly turbid, and precipitated after stirring for several hours (Supporting Information Figure S3 and for details see the Supporting Information Movie S1). In contrast, the MAAc precursors showed a negligible change in clarity and color under the same test, which indicates excellent stability of the MAAc precursor solution.[21,25] Although perovskite precursors are generally not heated for such a long time (~2 h) and placed in an inert atmosphere, this aging stress deteriorates the DMF/DMSO precursors when the stirring time is prolonged, or the solution is continuously heated.[16–19] Moreover, various organic PILs were synthesized (Supporting Information Figure S4), which could all completely dissolve 0.2 M $MAPbI_3$ to generate highly stable precursor colloids after being stored in air for 1 month.

To investigate the effect of the deterioration of perovskite precursors on the photovoltaic device performance, we constructed current density–voltage (J–V) curves of the best-performing devices based on DMF/DMSO (Supporting Information Figures S5a and S5c) and MAAc (Supporting Information Figures S5b and S5d) perovskite precursors solutions under continuous aging in air or heat in a glovebox. The precursor aging led to a significant decrease in the open circuit voltage (V_{oc}) and short-circuit current density (J_{sc}) of the solar cells obtained from the DMF/DMSO precursors solution. In contrast, there is negligible differences in the power conversion efficiencies of devices using the MAAc precursor solution, which indicates the good reproducibility of high-performance perovskite solar cells and excellent stability of the MAAc precursor solution.

In an ionic electrolyte, free ions act as charge carriers, and the redox reactions occur at the electrodes. These reactions are generally accompanied by the precipitation of the solid products.[26,27] To identify the characteristics of the precursor solution, we constructed an electrolytic cell system, as shown in Figure 2a. The current–voltage (C–V) cycling of the DMF/DMSO and MAAc perovskite precursor solutions (Figures 2b and 2c) and corresponding pure solvents (Supporting Information Figure S6) were compared under the same potential bias. An obvious voltage reduction from 0.3 to 0.15 V was observed in the redox reaction threshold of the DMF/DMSO precursor solution, indicating the unstable state of the ionic electrolyte. When PbI_2 and MAI were dissolved in the DMF/DMSO, an electrolyte with good ionic conductivity was formed. This led to a current approximately 40-fold higher than that of the pure solvent, indicating the presence of free and random ions in the solution.[27] However, the C–V cycling of MAAc precursor showed a negligible shift and no obvious redox reaction feature without difference due

DOI: 10.31635/ccschem.022.202101629
Citation: *CCS Chem.* **2022**, 4, 3264–3274
Link to VoR: https://doi.org/10.31635/ccschem.022.202101629

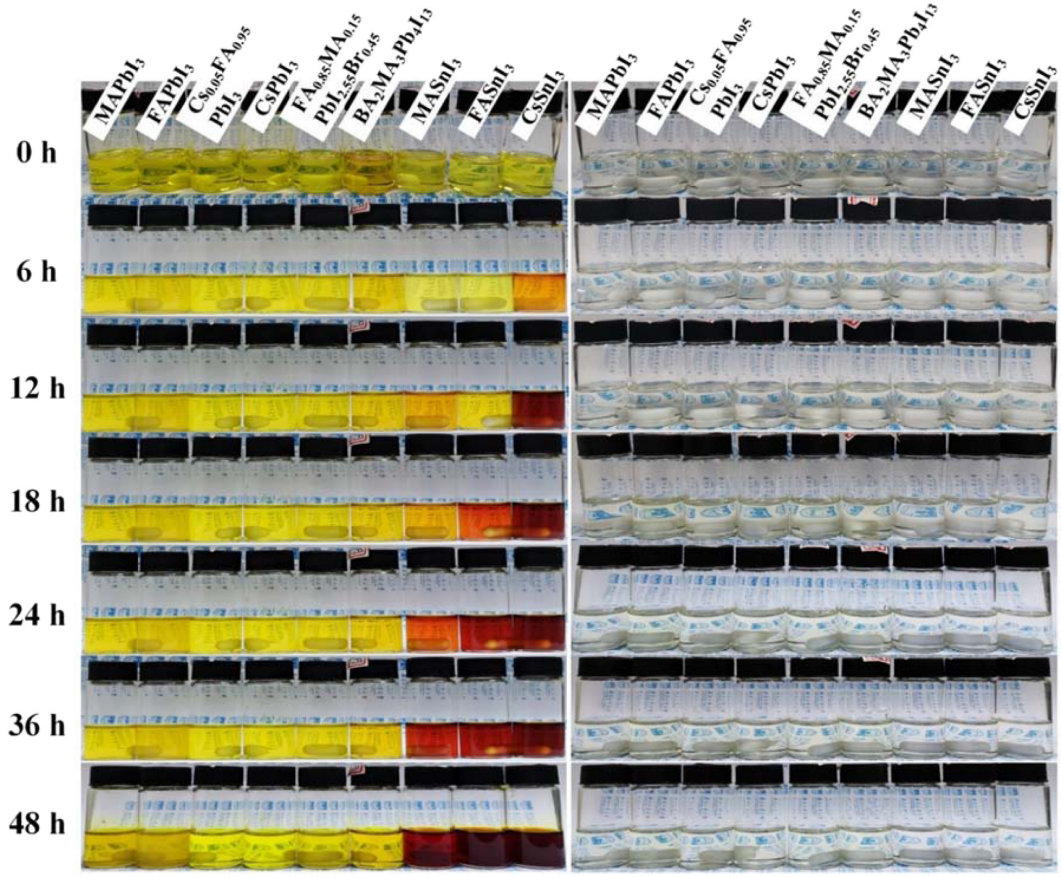

Figure 1 | *Perovskite colloids precursor solution behaviors of traditional solvent and PIL. Photographs of the perovskite precursor solutions with different compositional precursors ($MAPbI_3$, $FAPbI_3$, $Cs_{0.05}FA_{0.95}PbI_3$, $CsPbI_3$, $FA_{0.85}MA_{0.15}PbI_{2.55}Br_{0.45}$, $BA_2MA_3Pb_4I_{13}$, $MASnI_3$, $FASnI_3$, and $CsSnI_3$) in either MAAc (right) or DMF/DMSO (left) solvents with continuous aging in ambient environment.*

to the formation of stable, regularly distributed, and highly charged ion micelles. In addition, according to the long-term current–time (I–t) curve, the redox reaction current of the DMF/DMSO precursors was two orders of magnitude higher than that of the MAAc precursors (Figure 2d and Supporting Information Figure S7).

To quantify the migration and ion diffusion coefficients of precursors solutions, the electrochemical impedance spectroscopy (EIS) under different potential biases was also carried out. The free ion transfer and migration was faster and the redox reaction at the electrode was stronger under different potential biases in the DMF/DMSO precursors than in the MAAc precursors (Figures 2e and 2f). To gain further insight into the charge-transfer process from the precursor electrolyte to the electrode, the Mott–Schottky analysis was plotted as shown in Supporting Information Figures S8 and S9. The donor/acceptor density ($N_{D/A}$) was three orders of magnitude higher than that of the MAAc precursors, indicating the better electrochemical stability of the MAAc precursor. Furthermore, the electrochemical behavior of DMF/DMSO (Figure 2g) and MAAc (Figure 2h) precursors as electrolytes in electrolytic cells over a duration of 0–6 h under a potential bias of 0.6 V was observed (the electrochemical behavior under a potential bias of 1.5 V are shown in Supporting Information Figure S10). The DMF/DMSO precursors precipitated dendrite Pb compounds (Supporting Information Figures S11 and S12), suggesting Pb^{2+} and I^- ions existed in the original precursor, in which reduction of Pb^{2+} and I^- are the core reason for the deterioration of perovskite solution.[27] However, no significant change was observed in the MAAc precursor solution upon charging. These results indicate that despite various perovskite components, MAAc PIL protects them by forming regular enormous micelles with good electrochemical stability, thereby preventing cation reduction or anion oxidation.

Probing the coordination mechanism

The extremely high charge density in the ionic liquids leads to strong electrostatic shielding, which causes a decrease in the Coulomb repulsion. This interaction may be weaker than the van der Waals attraction.[28,29]

DOI: 10.31635/ccschem.022.202101629
Citation: *CCS Chem.* **2022**, 4, 3264–3274
Link to VoR: https://doi.org/10.31635/ccschem.022.202101629

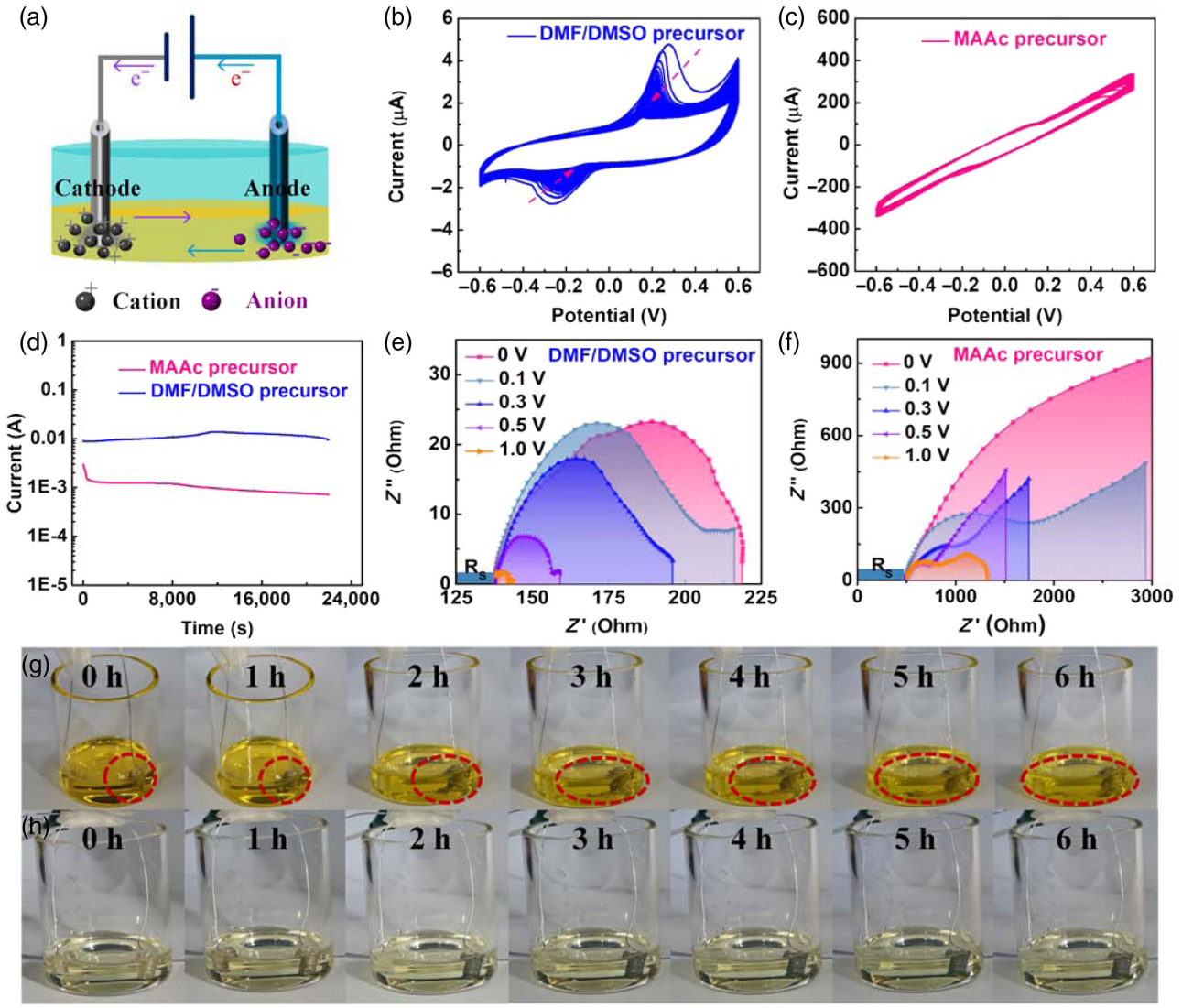

Figure 2 | *Electrochemical characteristics of the perovskite colloids precursor solutions. (a) Illustration of the electrolytic cell showing the redox reaction occurring in an ionic electrolyte. Cycling C–V curves of the DMF/DMSO (b) and MAAc (c) perovskite precursor solutions. The arrows indicate threshold shift of the redox reaction. (d) Relationship between the current (I) and reaction time (t) of the DMF/DMSO and MAAc perovskite precursor solutions. Alternating current (A.C.) EIS of the DMF/DMSO (e) and MAAc (f) perovskite precursors under different potential bias. Difference in the electrochemical behavior of the electrolytic cells using DMF/DMSO (g) and MAAc (h) precursors as electrolyte for durations from 0 to 6 h.*

To understand the origins of colloidal stabilization in the MAAc PIL, a series of experiments were conducted to characterize the interactions between the perovskite colloids and solvents. FTIR spectroscopy revealed that the stretching vibration of S=O in the pure DMF/DMSO solvent appeared at 1045 cm^{-1}, from which the wavenumber shifted to 1025 cm^{-1} for its precursor solution (Supporting Information Figure S13a).[17,18] In contrast, the stretching vibration peaks of the C=O in MAAc solvent were located at 1566.4 and 1005.2 cm^{-1}, while the corresponding peaks shifted to 1549.3 and 996.7 cm^{-1} in the MAAc precursor solution due to the coordination interaction with the Pb^{2+} ions (Supporting Information Figure S13b).[22,23] Moreover, the NMR spectroscopy further confirmed the formation of a stable colloidal precursor solution. The ^{1}H NMR spectra showed a stronger upfield chemical shift of the resonance signal of $-NH_3^+$ protons in the MAAc precursor (from 8.14 to 7.88 ppm) than in the DMF/DMSO precursor (from 7.55 to 7.44 ppm). This difference in the chemical shift is attributed to the stronger shielding effect of the N–H•••O=C–O^- hydrogen bond compared to the N–H•••I^- hydrogen bond (Figures 3a and 3b).[30,31] However, the ^{13}C chemical shift in the DMF/DMSO solvent and perovskite precursor

DOI: 10.31635/ccschem.022.202101629
Citation: *CCS Chem.* **2022**, 4, 3264–3274
Link to VoR: https://doi.org/10.31635/ccschem.022.202101629

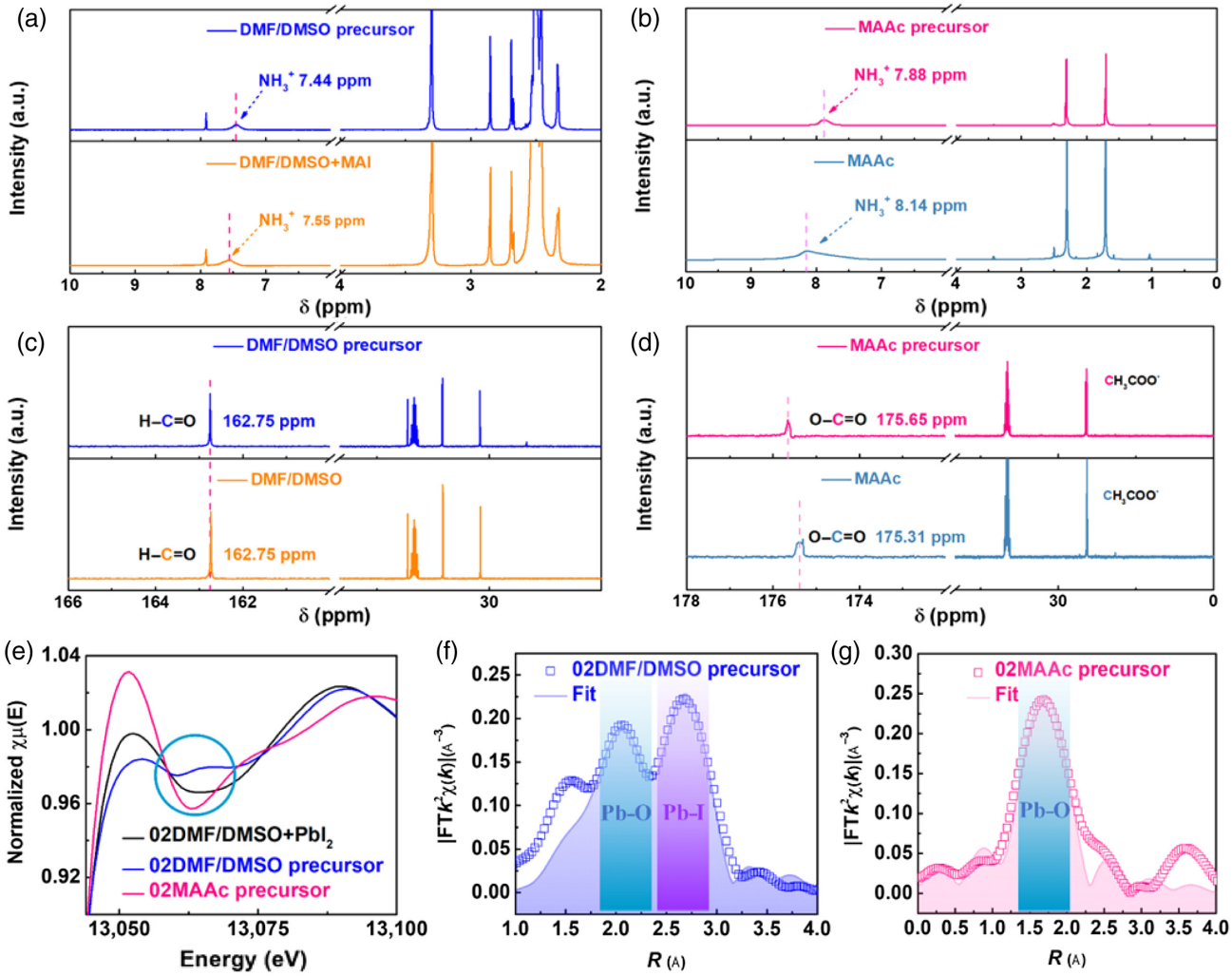

Figure 3 | *Probing the coordination mechanism of the perovskite colloids. The ^{1}H NMR spectra of DMF/DMSO (a) and MAAc (b) perovskite precursor solution with deuterated DMSO-d_6 at 295 K. Liquid-state ^{13}C NMR spectra of the C=O with DMF/DMSO (c) and MAAc (d) precursor colloid. The dash line indicates the shift of the asymmetric and symmetric stretching vibrations of the CH_3COO^- ion upon interaction with Pb^{2+} ion. (e) Normalized Pb XANES spectra of the Pb centers in all precursor samples. The absorption coefficient, μ, is a function of energy (E); χμ(E) is a function of E. The EXAFS spectra and fits in the R space observed on the Pb L-III edge of the precursor solution prepared using DMF/DMSO (f) and MAAc (g). χ(R) is the function of the interatomic distance R space.*

solutions did not significantly change. Meanwhile, the ^{13}C chemical shift changed from 175.31 ppm in pure MAAc to 175.65 ppm in the resultant colloidal precursor solution because of the strong binding between the O=C–O$^-$ and Pb^{2+} ions,[32–34] from which the lone pair electrons of O were attracted by Pb^{2+}, resulting in the decrease of electron density at the adjacent C atom and enhancement of the deshielding effect (Figures 3c and 3d). Although after long-term I-t measurement, the ^{1}H and ^{13}C NMR spectra still showed a similar chemical shift in the MAAc precursor (Supporting Information Figure S14).

Furthermore, the coordination chemistry of the Pb^{2+} ions in the precursor solutions was analyzed by XAFS on the Pb L-III edge (Figure 3e). The X-ray absorption near-edge structure spectroscopy (XANES) of the Pb L-III edge in the solutions confirmed that the Pb^{2+} ions coordinate with the I$^-$ ions in the DMF/DMSO solutions, which are labeled with a blue circle (Supporting Information Figure S15).[35,36] The coordination environment of the Pb^{2+} ions in the MAAc precursor solution was distinctly different from that in the DMF/DMSO solution according to the extended X-ray absorption fine structure spectroscopy (EXAFS). The Fourier transform (FT) curves of [$k^2\chi(k)$] are shown in Figures 3f and 3g. In the DMF/DMSO solution, a dominant peak at R = 2.98 Å was observed in the FT spectrum, which corresponds to the Pb-I scattering path (Supporting Information Figure S16). The MAI strongly impact the coordination number

DOI: 10.31635/ccschem.022.202101629
Citation: *CCS Chem.* **2022**, 4, 3264–3274
Link to VoR: https://doi.org/10.31635/ccschem.022.202101629

(CN) of Pb^{2+} ions as it varies from 2.4 ± 0.5 to 3.4 ± 0.5 in the DMF/DMSO perovskite precursor (Supporting Information Tables S1 and S2).[35,36] In addition, the secondary scatterings path appeared near R = 2.52 Å on the FT spectrum corresponding to the Pb–O scattering distance. However, in the MAAc precursor solution, the only peak on the FT spectrum was located at R = 2.31 Å. This corresponds to the Pb–O scattering path, which is hardly affected by the concentration and MAI (Supporting Information Figure S17).[37,38] To quantify the coordination effect, we fitted the coordination parameters of the Pb^{2+} ions using two paths from the PbI_2 -DMF structure.[39] The CN of the Pb^{2+} ions increased slightly from 1.6 ± 0.2 to 1.7 ± 0.4 as the MAAc precursor concentration increased from 0.2 to 0.4 M (Supporting Information Tables S3 and S4). Therefore, the R value in the MAAc was smaller than that in the DMF/DMSO, these results demonstrate that the coordination interaction of Ac^- ion is much stronger than DMF/DMSO, thereby forming a stable precursor component. Interestingly, the transformation of the coordination chemistry environment was directly observed via an intermolecular substitution process, which strongly indicates the variation of coordination interaction from Pb^{2+} and I to Pb^{2+} and O=C–O^-. (Supporting Information Figure S18 and Movie S2). These interactions determine that the robust precursor solution avoids the destruction by water and oxygen.[40]

Determining the interaction between perovskite colloids

The shapes and sizes of the micelles were measured at different concentrations using synchrotron SAXS. After background subtraction, the scattering plots showed similar SAXS patterns at a 0.2 M precursor concentration, which is typical for colloidal solutions (Figure 4a and Supporting Information Figure S19).[29,41] In comparison, a suspension of perovskite colloids in DMF/DMSO had a qualitatively different SAXS pattern from the cluster aggregates, with a pronounced peak at $q \approx 0.1$–0.8 Å, suggesting that the solution of DMF/DMSO was inhomogeneous.[28,34,39] Analysis using software, a program that enables the shape and size to be determined from SAXS data, showed that the irregularly orientated clusters are lamella-like with a mean thickness (d) of 5.12 nm, mean width (w) of 11.10 nm, and mean distance (L) of 16.22 nm between the lamellae in the DMF/DMSO (Figure 4b and inset).[42] This is in contrast with the MAAc gel-like lamellae, from which the mean thickness, width, and distance values of 34.69, 56.81, and 91.05 nm, respectively, were obtained with completely regular orientation (Figure 4c and inset, Supporting Information Table S5). In these ion clusters, Pb^{2+} ions are coordinated with acetate and surrounded by N–H•••I^- intermolecular hydrogen bonds interactions. Halide ions are protected by hydrogen bonds in ionic liquids, and amines are relatively isolated in this system until the solvent is removed. This is consistent with the results from dynamic light scattering (Supporting Information Figure S20), in which tens of nanometer-sized gel-like lamellae were monodispersed.[18,34,43]

An illustration of the distribution and interaction between the solvent and solute is shown in Figure 4d. The clusters aggregated as the concentrations increased in the DMF/DMSO. However, this process was different when the perovskite solvates were dissolved in the MAAc because of the strong coordination interaction and hydrogen bonding. These results confirm that the homogeneous structure of the micelles in the MAAc perovskite precursor was composed of colloids that are uniform in size, similar in shape, regular in orientation, and identical in nature. These stable micelles were formed without destruction of Pb^{2+} and I^- by coordination interaction, hydrogen bonding, and van der Waals forces, which leads to no obvious absorption of I_3^- and a strong emission peak around 575 nm (Supporting Information Figures S21 and S22).[21,27,37] TGA showed that MAAc can form a low boiling-point homogeneous precursor solution, which indicates that the faster evaporation of the solvent will also facilitate the supersaturation and accelerate the crystallization of perovskite (Supporting Information Figure S23).[27]

To gain further insights into the atomic mechanisms underlying the colloidal micelles, we performed first-principles MD simulations based on density functional theory on the chemical interaction between the PbI_2 crystal and MAAc PIL (Supporting Information Figure S24).[28,34] The strong-affinity Ac^- ions anchored to the dangling bond of Pb^{2+} in iodine-deficient PbI_2 via the electronic donor C=O, and it largely occupied the iodine positions in the PbI_2 crystal lattice (Figure 4e). The Pb^{2+} ions are effectively passivated by Ac^- through forming covalently bonded Pb–O bonds which further displaces other iodides in the proximity. This agrees with the XAFS and SAXS spectra.[37,38] In particular, the adsorption energy (E_a) per molecule above iodine vacancy of PbI_2 shows that up to three acetate ions participate in the coordination, which means that the Pb–O binding is strongest (Supporting Information Table S6). The existence of acetate can promote the infinite transformation of PbI_2 structure to PbAc liquid phase structure, and finally form stable PbAc liquid composite structures. We generated a model of composite structure with iodides replaced by acetate and found that this structure remained stable at 300 K.[44] The hybrid is stable according to the stable energy in our MD simulations (Supporting Information Figure S25). We observed that Ac^- ions drive and stabilize the formation of PbAc composite liquid structures upon coordination formation, which in turn prevent the deterioration of perovskite precursors.[39,45] N–H•••O=C–O^- hydrogen bonds and van der Waals forces further stabilized this structure as tens of

DOI: 10.31635/ccschem.022.202101629
Citation: *CCS Chem.* **2022**, 4, 3264–3274
Link to VoR: https://doi.org/10.31635/ccschem.022.202101629

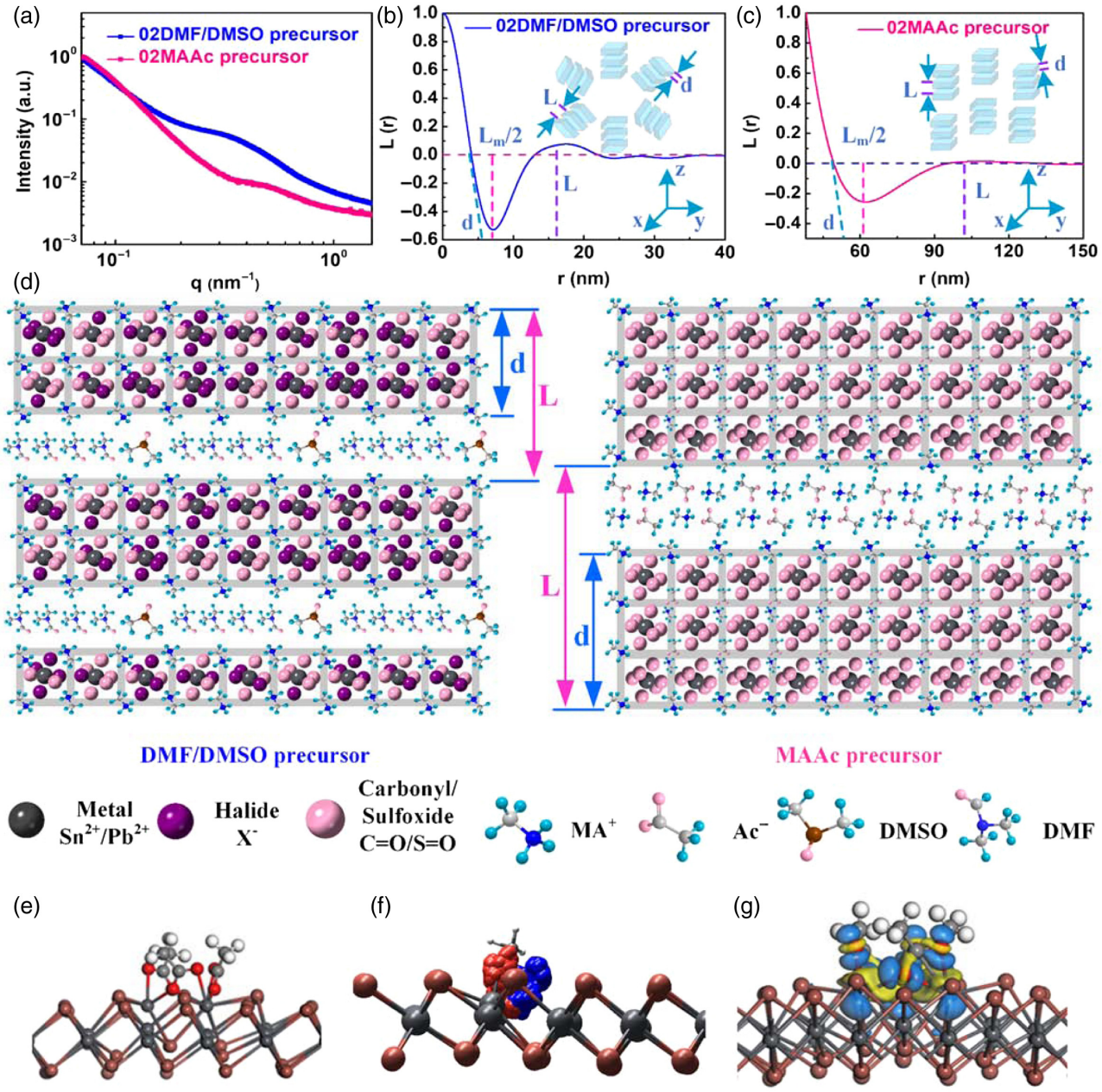

Figure 4 | *Determining the interaction between perovskite colloids using traditional solvent and ionic liquid. (a) SAXS intensity of the perovskite precursor colloids. I, scattering intensity; q, scattering vector. Fitting of the precursor colloids distribution in (b) DMF/DMSO and (c) MAAc with a one-dimensional correlation function model with and without irregular orientation, respectively. Inset shows the schematic of the distribution of the lamellar structures with a mean thickness (d), and width of the micelle region (w), mean distance between the lamellas (long period, L), and maximum distance between the lamellas, L_m. (d) Illustration of the distribution and interaction between the solvent and solute (DMF/DMSO, left; MAAc, right). (e) Side view of the strong adsorptions of three Ac^- ions above single iodine vacancy site. (f) Side view of the MDs trajectories of the two oxygen atoms of the Ac^- ion adsorbed at the iodine vacancy site simulated under 300 K. (g) Side view of the differential charge density plot. The yellow (blue) color indicates the charge loss (accumulation) of electrons upon adsorbing Ac^{-1} ions at iodine vacancy.*

nanometers colloids via regularly oriented gel-like lamellae (Supporting Information Figure S26). Detailed analysis of the projected MD trajectories shows that the oxygen atoms of acetate always rotate around the Pb atom during the whole MD process (Figure 4f). Top and side views of the trajectories and displacements of the two oxygen atoms of the Ac^- ion adsorbed at the iodine vacancy site are shown in Supporting Information Figure

DOI: 10.31635/ccschem.022.202101629
Citation: *CCS Chem.* **2022**, 4, 3264–3274
Link to VoR: https://doi.org/10.31635/ccschem.022.202101629

S27, which reveals that the motion of the Ac^- ion is always stabilized in a region of 3 Å around the Pb atoms (Movies S3 and S4). Such a strong chemical interaction was accompanied by a prominent charge transfer and state hybridization when the Pb coordinated with acetate; the electronic states of the oxygen atom were delocalized and transferred to the neighboring Pb atom, which essentially accounts for the stability of the precursor (Figure 4g and Supporting Information Figure S28).

Conclusions

We demonstrated the successful application of an environmentally friendly alternative organic PIL MAAc in obtaining stable metal halide perovskite precursors and high-performance solar cells under heat stress, air aging, and electrolytic dissociation. Through probing the coordination mechanism of the perovskite colloids in precursor solutions, we found that the presence of complete regular-orientated gel-like colloids lamellae, of tens of nanometers in size, in the MAAc instead of traditional DMF/DMSO solvent was confirmed. These colloids combined in the precursor solution through O=C–O^- and Pb^{2+} coordination interaction, N–H•••O=C–O^- hydrogen bonds, and van der Waals forces. First-principles MD simulations indicate that the Ac^- anions can promote the formation and stabilization of precursor colloids solution via the above interactions. Therefore, the PIL solvents can potentially facilitate the boost of many perovskite-based (such as lead-free, low-dimensional) photovoltaic, lasers, thin film transistors, detectors, LEDs, and other optoelectronic devices.

Supporting Information

Supporting Information is available and includes experimental procedures, Figures S1–S28, Tables S1–S6, and Movies S1–S4.

Conflict of Interest

There is no conflict of interest to report.

Acknowledgments

We thank beamline 1W1B and 1W2A staff at the Beijing Synchrotron Radiation Facility (BSRF) for providing the beamline; this work was performed in part at the High-Performance Computing Cluster (HPCC), which is supported by the Information and Communication Technology Office (ICTO) of the University of Macau. This work was financially supported by the Natural Science Foundation of China (grant nos. 51602149, 61705102, 61605073, 61935017, 62175268, and 22022309), the Macau Science and Technology Development Fund (grant no. FDCT-0044/2020/A1), research grants (grant nos. MYRG2018-00148-IAPME and MYRG2020-00151-IAPME) from the University of Macau and Natural Science Foundation of Guangdong Province, China (grant no. 2019A1515012186), Guangdong-Hong Kong-Macao Joint Laboratory of Optoelectronic and Magnetic Functional Materials (grant no. 2019B121205002), Shenzhen-Hong Kong-Macao Science and Technology Innovation Project (Category C) (grant no. SGDX2020110309360100), and the Young 1000 Talents Global Recruitment Program of China.

References

1. Yoo, J. J.; Seo, G.; Chua, M. R.; Park, T. G.; Lu, Y.; Rotermund, F.; Kim, Y.-K.; Moon, C. S.; Jeon, N. J.; Correa-Baena, J.-P. Efficient Perovskite Solar Cells via Improved Carrier Management. *Nature* **2021**, *590*, 587–593.
2. Xu, W.; Hu, Q.; Bai, S.; Bao, C.; Miao, Y.; Yuan, Z.; Borzda, T.; Barker, A. J.; Tyukalova, E.; Hu, Z. Rational Molecular Passivation for High-Performance Perovskite Light-Emitting Diodes. *Nat. Photon.* **2019**, *13*, 418–424.
3. Xing, G.; Mathews, N.; Lim, S. S.; Yantara, N.; Liu, X.; Sabba, D.; Grätzel, M.; Mhaisalkar, S.; Sum, T. C. Low-Temperature Solution-Processed Wavelength-Tunable Perovskites for Lasing. *Nat. Mater.* **2014**, *13*, 476–480.
4. Yu, W.; Li, F.; Yu, L.; Niazi, M. R.; Zou, Y.; Corzo, D.; Basu, A.; Ma, C.; Dey, S.; Tietze, M. L. Single Crystal Hybrid Perovskite Field-Effect Transistors. *Nat. Commun.* **2018**, *9*, 1–10.
5. Saidaminov, M. I.; Adinolfi, V.; Comin, R.; Abdelhady, A. L.; Peng, W.; Dursun, I.; Yuan, M.; Hoogland, S.; Sargent, E. H.; Bakr, O. M. Planar-Integrated Single-Crystalline Perovskite Photodetectors. *Nat. Commun.* **2015**, *6*, 1–7.
6. O'regan, B.; Grätzel, M. A Low-Cost, High-Efficiency Solar Cell Based on Dye-Sensitized Colloidal TiO_2 Films. *Nature* **1991**, *353*, 737–740.
7. Graetzel, M.; Janssen, R. A.; Mitzi, D. B.; Sargent, E. H. Materials Interface Engineering for Solution-Processed Photovoltaics. *Nature* **2012**, *488*, 304–312.
8. Kojima, A.; Teshima, K.; Shirai, Y.; Miyasaka, T. Organometal Halide Perovskites as Visible-Light Sensitizers for Photovoltaic Cells. *J. Am. Chem. Soc.* **2009**, *131*, 6050–6051.
9. Manser, J. S.; Kamat, P. V. Band Filling with Free Charge Carriers in Organometal Halide Perovskites. *Nat. Photon.* **2014**, *8*, 737–743.
10. Xing, G.; Mathews, N.; Sun, S.; Lim, S. S.; Lam, Y. M.; Grätzel, M.; Mhaisalkar, S.; Sum, T. C. Long-Range Balanced Electron- and Hole-Transport Lengths in Organic-Inorganic $CH_3NH_3PbI_3$. *Science* **2013**, *342*, 344–347.
11. Stranks, S. D.; Eperon, G. E.; Grancini, G.; Menelaou, C.; Alcocer, M. J.; Leijtens, T.; Herz, L. M.; Petrozza, A.; Snaith, H. J. Electron-Hole Diffusion Lengths Exceeding 1 Micrometer in an Organometal Trihalide Perovskite Absorber. *Science* **2013**, *342*, 341–344.
12. Li, L.; Chen, Y.; Liu, Z.; Chen, Q.; Wang, X.; Zhou, H. The Additive Coordination Effect on Hybrids Perovskite

DOI: 10.31635/ccschem.022.202101629
Citation: *CCS Chem.* **2022**, 4, 3264–3274
Link to VoR: https://doi.org/10.31635/ccschem.022.202101629

Crystallization and High-Performance Solar Cell. *Adv. Mater.* **2016**, *28*, 9862–9868.
13. Lee, J.-W.; Dai, Z.; Lee, C.; Lee, H. M.; Han, T.-H.; De Marco, N.; Lin, O.; Choi, C. S.; Dunn, B.; Koh, J. Tuning Molecular Interactions for Highly Reproducible and Efficient Formamidinium Perovskite Solar Cells via Adduct Approach. *J. Am. Chem. Soc.* **2018**, *140*, 6317–6324.
14. Noel, N. K.; Habisreutinger, S. N.; Wenger, B.; Klug, M. T.; Hörantner, M. T.; Johnston, M. B.; Nicholas, R. J.; Moore, D. T.; Snaith, H. J. A Low Viscosity, Low Boiling Point, Clean Solvent System for the Rapid Crystallisation of Highly Specular Perovskite Films. *Energy Environ. Sci.* **2017**, *10*, 145–152.
15. Jeon, N. J.; Noh, J. H.; Kim, Y. C.; Yang, W. S.; Ryu, S.; Seok, S. I. Solvent Engineering for High-Performance Inorganic–Organic Hybrid Perovskite Solar Cells. *Nat. Mater.* **2014**, *13*, 897–903.
16. Ahn, N.; Son, D.-Y.; Jang, I.-H.; Kang, S. M.; Choi, M.; Park, N.-G. Highly Reproducible Perovskite Solar Cells with Average Efficiency of 18.3% and Best Efficiency of 19.7% Fabricated via Lewis Base Adduct of Lead (II) Iodide. *J. Am. Chem. Soc.* **2015**, *137*, 8696–8699.
17. Yan, K.; Long, M.; Zhang, T.; Wei, Z.; Chen, H.; Yang, S.; Xu, J. Hybrid Halide Perovskite Solar Cell Precursors: Colloidal Chemistry and Coordination Engineering Behind Device Processing for High Efficiency. *J. Am. Chem. Soc.* **2015**, *137*, 4460–4468.
18. Ball, J. M.; Lee, M. M.; Hey, A.; Snaith, H. J. Low-Temperature Processed Meso-Superstructured to Thin-Film Perovskite Solar Cells. *Energy Environ. Sci.* **2013**, *6*, 1739–1743.
19. Nie, W.; Tsai, H.; Asadpour, R.; Blancon, J.-C.; Neukirch, A. J.; Gupta, G.; Crochet, J. J.; Chhowalla, M.; Tretiak, S.; Alam, M. A. High-Efficiency Solution-Processed Perovskite Solar Cells with Millimeter-Scale Grains. *Science* **2015**, *347*, 522–525.
20. Ren, H.; Yu, S.; Chao, L.; Xia, Y.; Sun, Y.; Zuo, S.; Li, F.; Niu, T.; Yang, Y.; Ju, H. Efficient and Stable Ruddlesden–Popper Perovskite Solar Cell with Tailored Interlayer Molecular Interaction. *Nat. Photon.* **2020**, *14*, 154–163.
21. Chao, L.; Xia, Y.; Li, B.; Xing, G.; Chen, Y.; Huang, W. Room-Temperature Molten Salt for Facile Fabrication of Efficient and Stable Perovskite Solar Cells in Ambient Air. *Chem* **2019**, *5*, 995–1006.
22. Saidaminov, M. I.; Spanopoulos, I.; Abed, J.; Ke, W.; Wicks, J.; Kanatzidis, M. G.; Sargent, E. H. Conventional Solvent Oxidizes Sn (II) in Perovskite Inks. *ACS Energy Lett.* **2020**, *5*, 1153–1155.
23. Leijtens, T.; Prasanna, R.; Gold-Parker, A.; Toney, M. F.; McGehee, M. D. Mechanism of Tin Oxidation and Stabilization by Lead Substitution in Tin Halide Perovskites. *ACS Energy Lett.* **2017**, *2*, 2159–2165.
24. Wei, H.; Chen, S.; Zhao, J.; Yu, Z.; Huang, J. Is Formamidinium Always More Stable Than Methylammonium? *Chem. Mater.* **2020**, *32*, 2501–2507.
25. Tsai, H.; Nie, W.; Lin, Y. H.; Blancon, J. C.; Tretiak, S.; Even, J.; Gupta, G.; Ajayan, P. M.; Mohite, A. D. Effect of Precursor Solution Aging on the Crystallinity and Photovoltaic Performance of Perovskite Solar Cells. *Adv. Energy Mater.* **2017**, *7*, 1602159.
26. Samu, G. F.; Balog, Á.; De Angelis, F.; Meggiolaro, D.; Kamat, P. V.; Janáky, C. Electrochemical Hole Injection Selectively Expels Iodide from Mixed Halide Perovskite Films. *J. Am. Chem. Soc.* **2019**, *141*, 10812–10820.
27. Wang, K.; Wu, C.; Hou, Y.; Yang, D.; Li, W.; Deng, G.; Jiang, Y.; Priya, S. A Nonionic and Low-Entropic MA $(MMA)_nPbI_3$-Ink for Fast Crystallization of Perovskite Thin Films. *Joule* **2020**, *4*, 615–630.
28. Zhang, H.; Dasbiswas, K.; Ludwig, N. B.; Han, G.; Lee, B.; Vaikuntanathan, S.; Talapin, D. V. Stable Colloids in Molten Inorganic Salts. *Nature* **2017**, *542*, 328–331.
29. Lanning, O. J.; Madden, P. A. Screening at a Charged Surface by a Molten Salt. *J. Phys. Chem. B* **2001**, *108*, 11069–11072.
30. Bi, D.; Yi, C.; Luo, J.; Décoppet, J.-D.; Zhang, F.; Zakeeruddin, S. M.; Li, X.; Hagfeldt, A.; Grätzel, M. Polymer-Templated Nucleation and Crystal Growth of Perovskite Films for Solar Cells with Efficiency Greater than 21%. *Nat. Energy* **2016**, *1*, 1–5.
31. Li, X.; Dar, M. I.; Yi, C.; Luo, J.; Tschumi, M.; Zakeeruddin, S. M.; Nazeeruddin, M. K.; Han, H.; Grätzel, M. Improved Performance and Stability of Perovskite Solar Cells by Crystal Crosslinking with Alkylphosphonic Acid ω-Ammonium Chlorides. *Nat. Chem.* **2015**, *7*, 703–711.
32. Wang, X.; Ran, X.; Liu, X.; Gu, H.; Zuo, S.; Hui, W.; Lu, H.; Sun, B.; Gao, X.; Zhang, J. Tailoring Component Interaction for Air-Processed Efficient and Stable All-Inorganic Perovskite Photovoltaic. *Angew. Chem. Int. Ed.* **2020**, *59*, 13354–13361.
33. Chao, L.; Niu, T.; Gu, H.; Yang, Y.; Wei, Q.; Xia, Y.; Hui, W.; Zuo, S.; Zhu, Z.; Pei, C. Origin of High Efficiency and Long-Term Stability in Ionic Liquid Perovskite Photovoltaic. *Research* **2020**, *30*, 2616345.
34. Liu, Z.; Shao, C.; Jin, B.; Zhang, Z.; Zhao, Y.; Xu, X.; Tang, R. Crosslinking Ionic Oligomers as Conformable Precursors to Calcium Carbonate. *Nature* **2019**, *574*, 394–398.
35. Tyson, T.; Gao, W.; Chen, Y.-S.; Ghose, S.; Yan, Y. Large Thermal Motion in Halide Perovskites. *Sci. Rep.* **2017**, *7*, 1–10.
36. Pan, J.; Mu, C.; Li, Q.; Li, W.; Ma, D.; Xu, D. Room-Temperature, Hydrochloride-Assisted, One-Step Deposition for Highly Efficient and Air-Stable Perovskite Solar Cells. *Adv. Mater.* **2016**, *28*, 8309–8314.
37. Sharenko, A.; Mackeen, C.; Jewell, L.; Bridges, F.; Toney, M. F. Evolution of Iodoplumbate Complexes in Methylammonium Lead Iodide Perovskite Precursor Solutions. *Chem. Mater.* **2017**, *29*, 1315–1320.
38. Xiong, J.; Koopal, L. K.; Tan, W.; Fang, L.; Wang, M.; Zhao, W.; Liu, F.; Zhang, J.; Weng, L. Lead Binding to Soil Fulvic and Humic Acids: NICA-Donnan Modeling and XAFS Spectroscopy. *Environ. Sci. Technol.* **2013**, *47*, 11634–11642.
39. Wakamiya, A.; Endo, M.; Sasamori, T.; Tokitoh, N.; Ogomi, Y.; Hayase, S.; Murata, Y. Reproducible Fabrication of Efficient Perovskite-Based Solar Cells: X-Ray Crystallographic Studies on the Formation of $CH_3NH_3PbI_3$ Layers. *Chem. Lett.* **2014**, *43*, 711–713.

DOI: 10.31635/ccschem.022.202101629
Citation: *CCS Chem.* **2022**, 4, 3264–3274
Link to VoR: https://doi.org/10.31635/ccschem.022.202101629

40. Pauling, L. The Dependence of Bond Energy on Bond Length. *J. Phys. Chem.* **1954**, *58*, 662–666.
41. Kamysbayev, V.; Srivastava, V.; Ludwig, N. B.; Borkiewicz, O. J.; Zhang, H.; Ilavsky, J.; Lee, B.; Chapman, K. W.; Vaikuntanathan, S.; Talapin, D. V. Nanocrystals in Molten Salts and Ionic Liquids: Experimental Observation of Ionic Correlations Extending Beyond the Debye Length. *ACS Nano* **2019**, *13*, 5760–5770.
42. Zhi-Hong, L. A Program for SAXS Data Processing and Analysis. *Chin. Phys. C* **2013**, *37*, 108002.
43. Liang, C.; Gu, H.; Xia, Y.; Wang, Z.; Liu, X.; Xia, J.; Zuo, S.; Hu, Y.; Gao, X.; Hui, W. Two-Dimensional Ruddlesden-Popper Layered Perovskite Solar Cells Based on Phase-Pure Thin-Films. *Nat. Energy* **2020**, *6*, 38–45.
44. Carignano, M. A.; Kachmar, A.; Hutter, J. Thermal Effects on $CH_3NH_3PbI_3$ Perovskite from Ab Initio Molecular Dynamics Simulations. *J. Phys. Chem. Lett.* **2015**, *119*, 8991–8997.
45. Lu, H.; Liu, Y.; Ahlawat, P.; Mishra, A.; Tress, W. R.; Eickemeyer, F. T.; Yang, Y.; Fu, F.; Wang, Z.; Avalos, C. E. Vapor-Assisted Deposition of Highly Efficient, Stable Black-Phase $FAPbI_3$ Perovskite Solar Cells. *Science* **2020**, *370*, eabb8985.

DOI: 10.31635/ccschem.022.202101629
Citation: *CCS Chem.* **2022**, 4, 3264–3274
Link to VoR: https://doi.org/10.31635/ccschem.022.202101629